JOURNAL OF AIRCRAFT
Vol. 32, No. 3, May–June 1995

Quantifiable Vortex Features of F-106B Aircraft at Subsonic Speeds

John E. Lamar* and Jay Brandon†
NASA Langley Research Center, Hampton, Virginia 23681
and
Thomas D. Johnson Jr.‡
Lockheed Engineering and Sciences Company, Inc., Hampton, Virginia 23666

Quantifiable vortex features and separated-flow origins have been determined on an F-106B aircraft at 1-*g* subsonic speeds using the vapor-screen technique coupled with image enhancement, photogrammetry, and computer graphics. In particular, the spatial location of vortex cores, their tracks over the wing, and the approximate reattachment locations have been determined as a function of angle of attack and Reynolds number. Increasing the Reynolds number generally delays or suppresses large-scale separation and promotes the formation of multiple vortices, whereas increasing the angle of attack generally promotes the formation of a single vortex system. The multiple vortices observed may likely be attributed to small surface distortions in the wing leading-edge region. Comparisons of off-surface determined vortex core location and reattachment point approximation from the vapor-screen technique are made with those from the on-surface techniques of static pressure and oil flow and show generally good agreement. A comparison between quantified vortex features from flight and wind tunnel showed reasonably good agreement over the forward part of the wing for angles of attack from 16 to 20 deg.

Nomenclature

$C_{p,u}$ = upper-surface static-pressure coefficient
c_r = theoretical root chord for F-106B, 35.63-ft full-scale
g = acceleration due to gravity
h = altitude, ft
l = inboard distance to vortex-system core from wing leading edge along light-sheet footprint, in., Fig. 9
M_∞ = freestream Mach number
R_n = Reynolds number based on wing reference chord of 23.75 ft
r = inboard distance to vortex-system reattachment point from wing leading edge along light-sheet footprint, in., Fig. 9
x/c_r = fractional distance along the theoretical root chord, positive aft
α = angle of attack, deg
Φ = light-sheet position angle, measured counterclockwise from fuselage nose as viewed from above, deg, Fig. 3

Introduction

VORTEX features of an F-106B aircraft were experimentally determined from results recorded during a flight test conducted in 1991 and were subsequently documented in Ref. 1. A summary of the subsonic 1-*g* results is presented in this article from both off- and on-surface data obtained with a variety of new and old techniques. The new techniques include a rotating vapor-screen coupled with image enhancement, photogrammetry, and computer graphics. This new use of the vapor-screen technique, first described in concept form in Ref. 2, provides off-surface coverage over most of the wing upper-surface. These techniques are both two and three dimensional and assist in the identification of key vortex features from the images. The old techniques are on-surface and include both pressure and oil flow.

The reason for performing this flight test was to understand the origination of multiple primary (corotating) vortices unexpectedly found in a previous test (1985), and reported in Ref. 3, above this 60-deg delta wing over a range of moderate α. Corotating vortices have been reported as streamwise vortices at supersonic speeds and low α on flat and cambered models[4] and on aircraft in flight under loaded conditions.[5] However, it is not clear that these are the same phenomenon as that under investigation. Figure 1 shows three models for corotating vortex development on the F-106B aircraft. Figure 1a is from Ref. 6 and is based on the fixed-light-sheet results of the 1985 test, whereas the other two models are based on the 1991 flight results.

Description of Test Hardware and Flight Experiment

Aircraft

The F-106B aircraft is a two-place supersonic all-weather interceptor. It has an area-ruled fuselage, a 60-deg delta wing of aspect ratio 2.20, and uses elevons instead of a conventional aileron-elevator arrangement, as shown in Fig. 2. The wing has a modified conical camber in the leading-edge region and a small leading-edge radius. This figure shows the overall dimensions of the aircraft as well as reference values for fuselage station (FS), butt line (BL), and waterline (WL). Figure 2 is also used to illustrate that the wing leading-edge region is composed of many pieces and has a slot. Some of these pieces, called access straps, bridge leading-edge access areas between major segments located ahead of the no. 1 spar. The

Presented as Paper 93-3471 at the AIAA 11th Applied Aerodynamics Conference, Monterey, CA, Aug. 9–11, 1993; received April 29, 1994; revision received Aug. 26, 1994; accepted for publication Aug. 26, 1994.

*Senior Research Scientist, Vehicle Performance Branch, M/S 247. Associate Fellow AIAA.
†Aerospace Engineer, Vehicle Dynamics Branch, M/S 355. Senior Member AIAA.
‡Principal Engineer, Aerodynamics, 144 Research Dr. Senior Member AIAA.

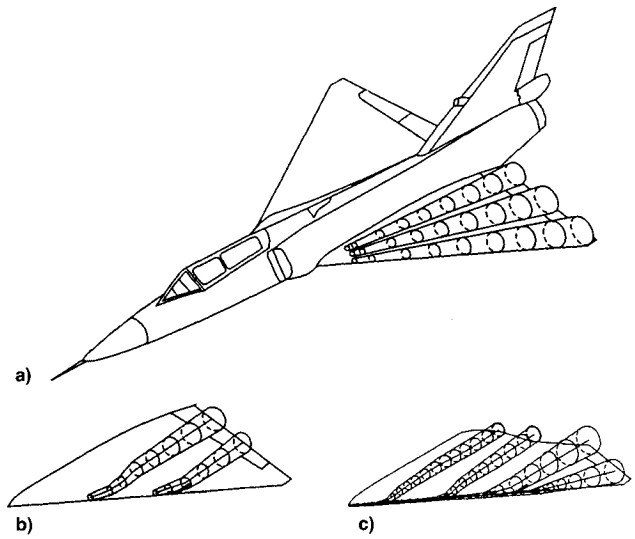

Fig. 1 Three models for origination of multiple vortex systems on F-106B wing, based on a) 1985 flight vapor screen, b) 1991 flight vapor screen, and c) 1991 flight oil flow.

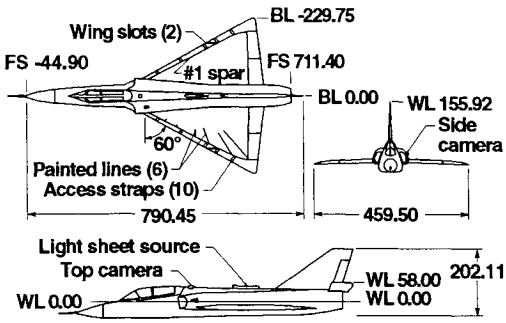

Fig. 2 Three-view sketch of F-106B aircraft. Dimensions are in inches unless otherwise noted.

slot acts as a boundary-layer fence to laterally constrain the flow.

The aircraft was extensively instrumented to measure and record onboard parameters associated with the vapor-screen system, the aircraft motion, surface static pressures, and the surrounding environment. The left wing was used for both the vapor-screen and oil-flow visualization techniques. In order to improve the visual contrast of the recorded images, the wing was painted flat black. Figure 2 shows vapor-screen reference lines on the left wing (white lines painted on the aircraft), which were located where the light sheet crossed the upper surface at Φ = 43, 63, 93, 108, 123, and 130 deg.

Figure 3 shows the left-wing slot beginning at Φ = 103 deg and the approximate wing regions over which the seeding and light-sheet systems are mutually effective. Note that the lateral extent of the seeded flow is inboard of the slot. The right wing was reserved for surface pressure measurements, and Fig. 3 also shows the relationship between the 30 static-pressure ports contained within the four pressure belt-sets used in this test and the left-wing light-sheet angles reflected about the centerline.

Vapor-Screen Systems

In this flight test the vapor-screen technique involved the use of systems that were conceptually the same as those for the 1985 test[3]: propylene glycol vapor for seeding, mercury-arc light sheet for flowfield illuminating, and video system for image recording. However, there were specific changes made in order to accomplish the objectives of the current test and these are described in Ref. 1. Some of the hardware changes included light sheet relocation and side camera addition. (This

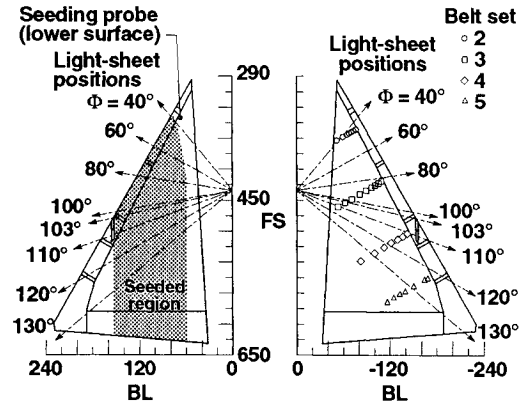

Fig. 3 Regions of wing covered by seeding and light-sheet systems (left wing), and pressure port locations on right wing relative to left-wing light-sheet angles reflected about centerline.

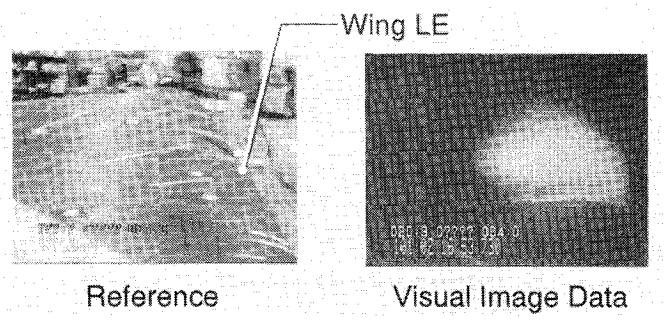

Fig. 4 Sample of reference wing upper-surface and basic visual image data from top camera.

camera addition was made in order to record images over the forward part of the wing.) A sample of the reference wing upper-surface and basic visual image data from the top camera is presented in Fig. 4.

Flight-Test Experiment

The flight-test experiment, composed of both 1 g and loaded maneuvers, was conducted so as to obtain as much vapor-screen image data as possible on each of five night flights. The test parameters were α, M_∞, R_n, and load factor. Variations of R_n with α were accomplished by flying a subsonic 1-g deceleration maneuver at constant altitudes between 15,000–35,000 ft in approximately 10,000-ft increments, with α ranging from 13 to 22 deg. There are two causes for the R_n variation associated with this maneuver: the decrease in atmospheric density with increasing altitude and the speed reduction required in order to maintain 1-g flight while increasing α. Each nominal altitude had a range of R_n associated with it and this is referred to subsequently as a set.

For all maneuvers, the best vapor-screen contrast was obtained by flying at night with the aircraft position lights off, the moon down, and away from ground-based lights. Angle-of-attack variation during data taking was about $\pm$0.5 deg.

Discussion of Flight Results

This section describes the use of vapor-screen images to help clarify the origination of corotating vortices; provides a brief description of techniques used on the images to determine vortex features; discusses sample results and the effect of Reynolds number; and provides comparisons with surface pressure, surface oil-flow, and wind-tunnel results.

Corotating Vortex Origination

Since the origination of the corotating vortices is tied in with the flow over the forward part of the wing, side-camera images have been selected to study the process. Figure 5 presents the results at M_∞ = 0.29 and α = 17.8 deg. The

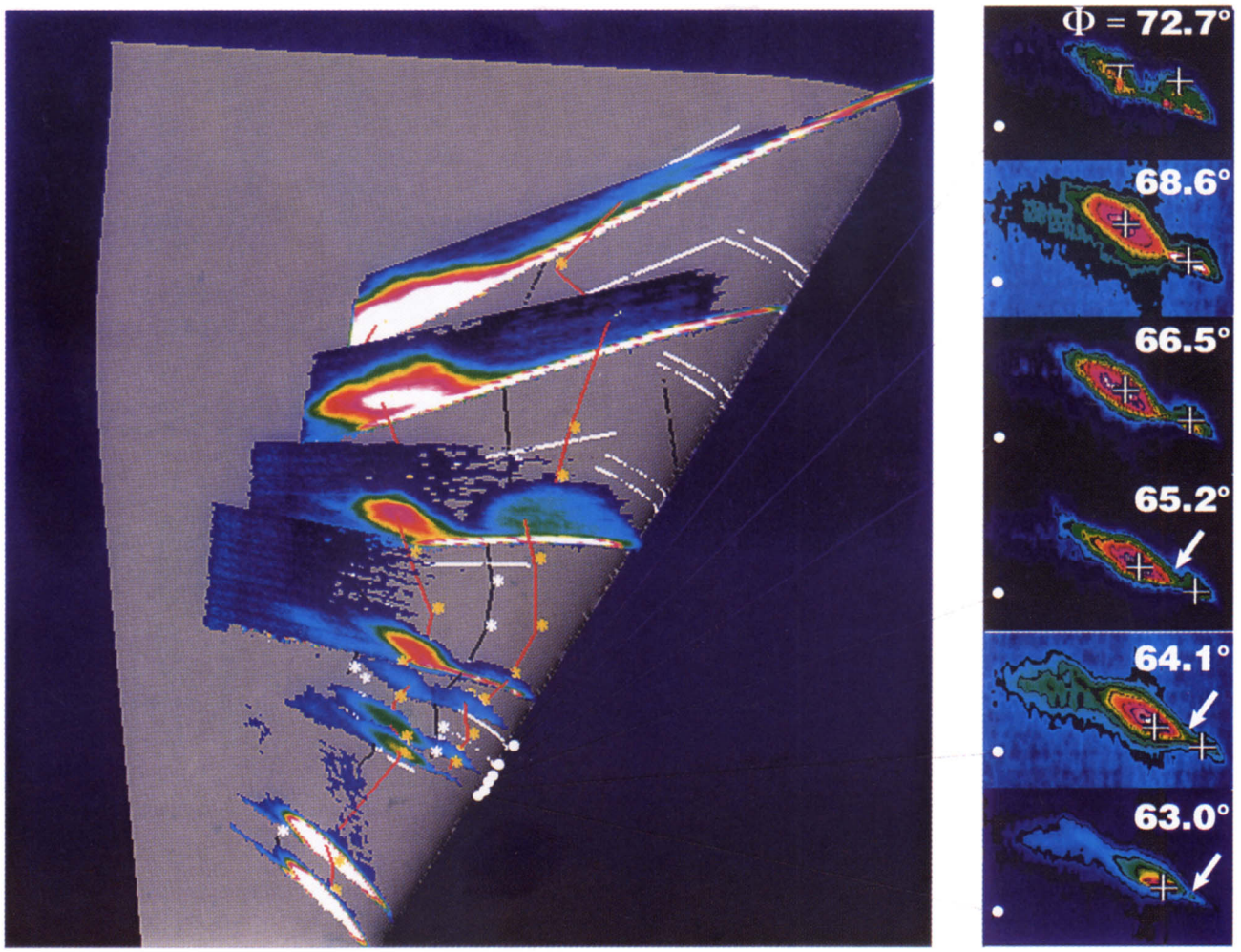

Fig. 5 Three-dimensional perspective of vortex systems over surface geometry and two-dimensional cuts of enhanced vortex systems showing the multiple vortex growth process for α = 17.8 deg, nominal 15,000 ft altitude, and M_∞ = 0.3. (Vapor-screen determined cores are connected by red lines with * and reattachment points by black lines with *; two-dimensional vortex core indicated by plus sign; reflex denoted by ↙.)

right-hand portion of this figure shows that with increasing light-sheet angle ($\Phi > 63$ deg) the core, or bright centroid, moves from outboard to inboard within the vortex envelope. This movement is construed as the vortex system changing from a leading-edge separation bubble type to the more classical off-surface type. From Ref. 7 the transition in vortex type can be computed—based on sharp-edged, cambered, delta-wing test results—and it should occur near α = 9 deg at M_∞ = 0.29 for a 60-deg delta wing. In the current test the vortex systems did not become visible until $\alpha \approx 13$ deg. The higher α required here are likely associated with two factors: 1) the inexact transition boundary at this low value of M_∞ and 2) the round, not sharp, leading edge (LE) on this F-106B aircraft.

Moreover, the vortex envelope develops a reflexive region near the LE. As the centroid moves inboard, the reflex becomes more accentuated toward the LE (Fig. 5). Outboard of this region a second vortex system emerges for $\Phi \geq 64.1$ deg, as shown in Fig. 5. Hence, multiple vortex-system origination is tied in with the inboard shift of the core at the lower angles of attack and a related envelope change. These changes could be caused by a phenomenon associated with a vortex-sheet tearing process,[8,9] either fluid dynamic or brought about by some aspect of the aircraft geometry.

The left-hand portion of Fig. 5 shows a collection of images from both side and top cameras, along with the vortex-core and reattachment-point lines displayed on the wing using the software package flow analysis and software toolkit (FAST).[10] This figure shows the process of vortex formation and aft migration or shedding over the wing. In particular, as one vortex is shed aft over the wing, it is followed by the formation of another and more outboard vortex system that is shed aft, etc. This forms the basis of the model shown in Fig. 1b.

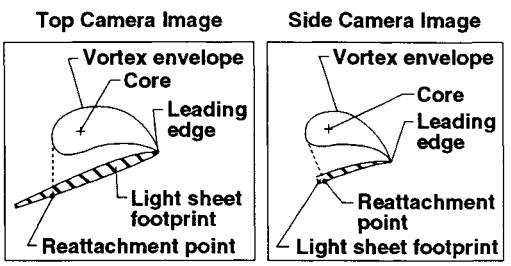

Fig. 6 Illustration of reattachment-point location using a computer software (graphics) procedure.

Vortex Feature Determination Techniques

This section describes how the vortex-core and reattachment-point lines are determined from two-dimensional enhanced basic-visual-data. The core locations, illustrated in Fig. 5, are determined by computer software that calculates a weighted average of the gray scale values of the reflected light in a user controlled, circumscribed region. The preceding was done because this cambered wing (with its round leading edge) tends to produce a diffuse vortex system, one in which the propylene glycol condensed particles do not revaporize in the core, but merely concentrate.[1] The determined location from this process is a centroid and is called the vortex core.

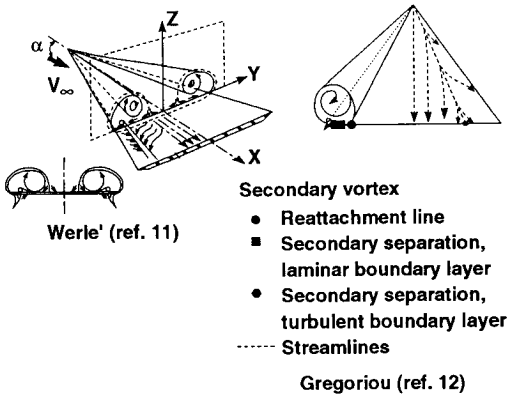

Fig. 7 Representative sketches of off-surface vortex systems and associated surface flow.

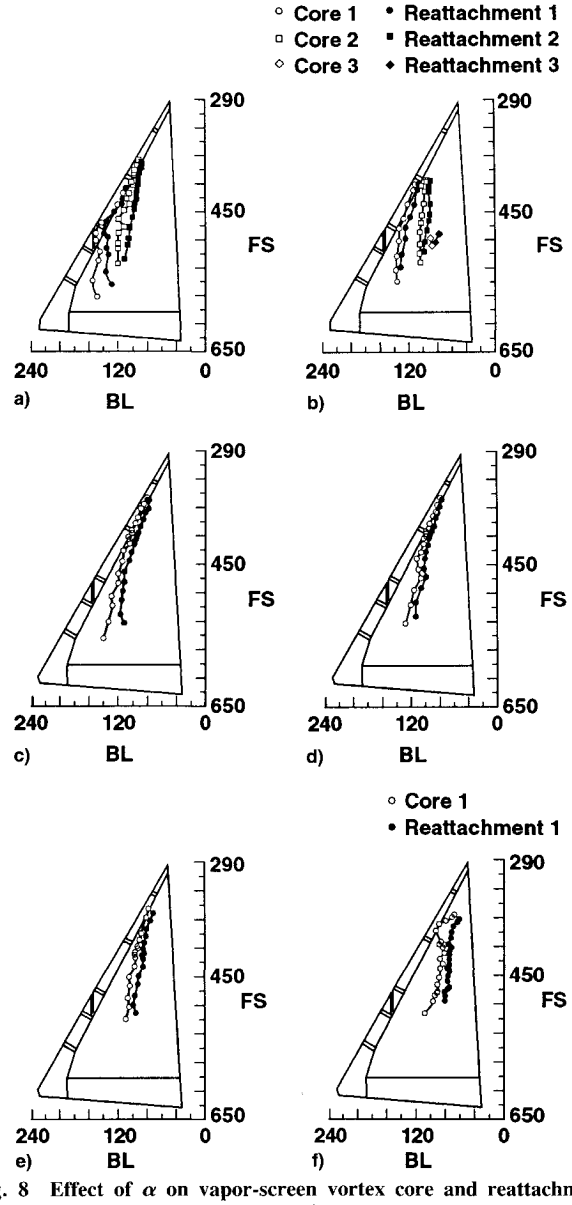

Fig. 8 Effect of α on vapor-screen vortex core and reattachment tracks at nominal altitude of 25,000 ft and 1 g. α = a) 13.9, b) 14.9, c) 16.1, d) 17.0, e) 18.8, and f) 22.5 deg.

Using vapor-screen data to find an approximation of the reattachment point is not as straightforward, because, as shown in Fig. 6, the vapor particles provide only an envelope or filled outline of the vortex system. For results presented here, the core-locating software has been applied to determine the most inboard edge (inner extent) of the envelope. By projecting this portion of the vortex envelope to the wing upper surface, a track of the inboard extreme can be established. This surface location of the inner extent of the envelope can be used as an approximation of the reattachment point. The rational for this statement is based on a study of Fig. 7 (from Refs. 11 and 12). This led to a hypothesis that the lateral difference between the projected vortex envelope and reattachment point is small. Further discussions regarding this technique and potential sources of errors for determining the reattachment point using off-surface flow visualization data are included in Ref. 1.

Even with potential sources of error, this technique still provides a rational basis for estimating the reattachment location in those situations where surface techniques are not available. Comparisons with oil-flow results are presented in an attempt to gauge the reliability of this technique.

The resulting vortex-system core location(s) and reattachment point(s) for each image can be located in three-dimensional space through the process of photogrammetry, as described in Ref. 1. Hence, these results can be displayed as surface tracks mapped onto the wing planform, and also in terms of distance to the leading edge along the light sheet at its Φ. Examples are given next.

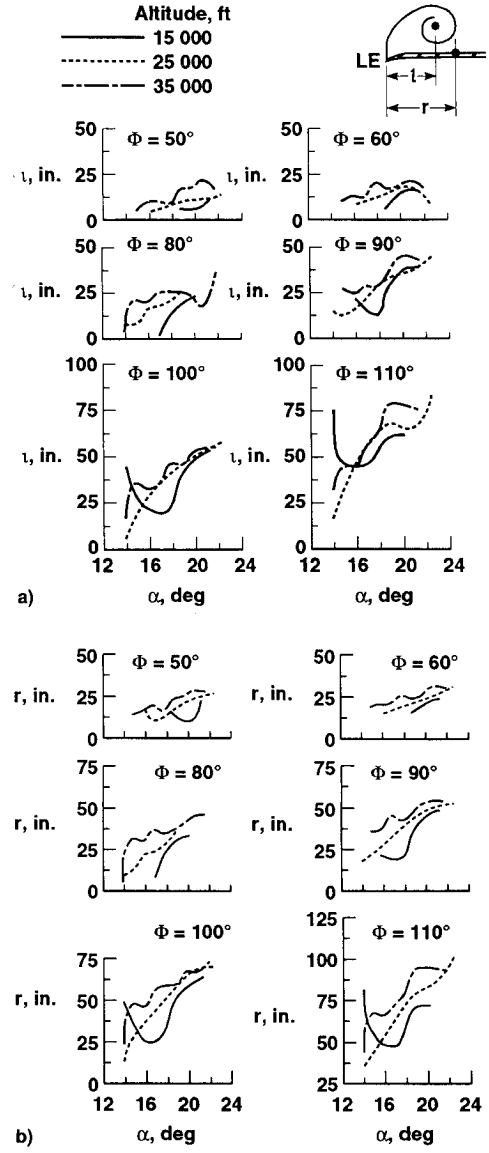

Fig. 9 Effect of altitude on distance from outermost (vapor-screen) vortex-system features to local leading edge along light-sheet ray at 1 g a) core distance and b) reattachment point distance.

Vortex Features Projected to Surface

Surface Tracks

Figure 8 presents vortex-system core- and reattachment-point surface tracks graphed onto the plan view of the left wing over an angle-of-attack range at a nominal 25,000 ft altitude. This figure shows that increasing angle of attack generally reduces the number of discernible vortex systems from as many as three to one, above $\alpha = 14.9$ deg, and there is an overall inboard vortex system movement. Given the fact that multiple primary vortices were known to exist on this wing, these results are not surprising.

These results are also consistent with the delay in significant separation associated with flights at higher Reynolds numbers. In particular, the R_n associated with the 25,000-ft-altitude flights range from 35.1×10^6 at the lowest α to 26.6×10^6 at the highest.

At some angles of attack the additional vortex systems seem to either point to one of the straps or be influenced by it in some way. Thus, one likely source of the multiple vortices observed in flight is the disturbances associated with these access straps. Note in particular from Fig. 3 that there is a strap near $\Phi = 70$ deg.

Reynolds Number Effect

Figures 9a and 9b generally show, for the outermost vortex system, similar effects of altitude on core and reattachment point distance to the local leading edge (l and r, respectively) for the various light-sheet angles over the angle-of-attack range. The general trend of l and r is to be displaced inboard over the middle α range with increasing altitude. The altitude increase is always associated with a lower Reynolds number set.[1] The inboard movement is reasonable because of flow separation and vortex merging occurring at the lower α for the lower R_n set. This effect of lower R_n promotes a single vortex at moderate α. Furthermore, the system is likely to be larger, and to have its core and reattachment locations more inboard. Conversely, for the highest R_n set (lowest altitude group), a delay occurs in the separation process leading to vortex formation. This results in the more likely formulation of a multiple vortex system, and also results in a more inboard position of the core and reattachment locations for the outermost vortex.

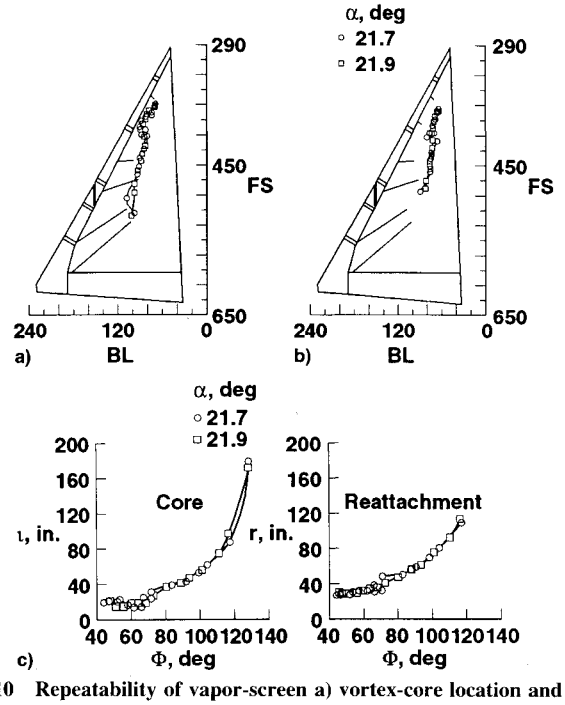

Fig. 10 Repeatability of vapor-screen a) vortex-core location and b) reattachment point at nominal altitude of 35,000 ft, $\alpha = 21.8$ deg, 1 g, and $M_\infty = 0.4$; c) variation of l and r with Φ.

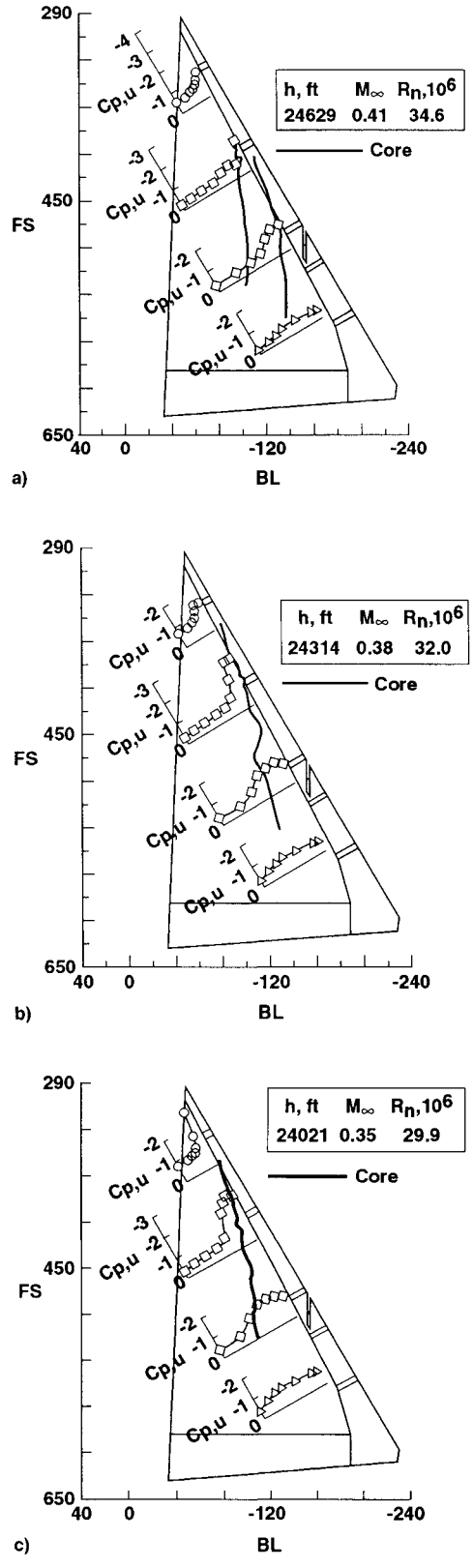

Fig. 11 Superposition of vapor-screen vortex-core tracks on surface pressures at nominal 1 g. α = a) 14.9, b) 17.0, and c) 18.8 deg.

Error Assessment

To help assess some of the errors identified in Ref. 1, a repeatability check for the top camera was done by comparing the data of $\alpha = 21.9$ deg with those of $\alpha = 21.7$ deg. The results are shown in Figs. 10a and 10b. The general agreement for both the vortex-core and the reattachment-point surface tracks is quite good, with maximum local lateral errors of 11

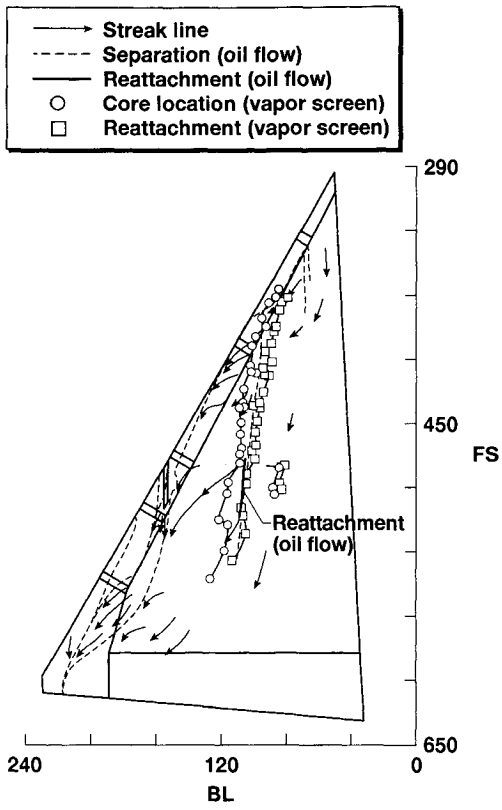

Fig. 12 Superposition of vortex-system vapor-screen results on oil-flow patterns at nominal altitude of 15,000 ft, α = 19 deg, and M_∞ = 0.3.

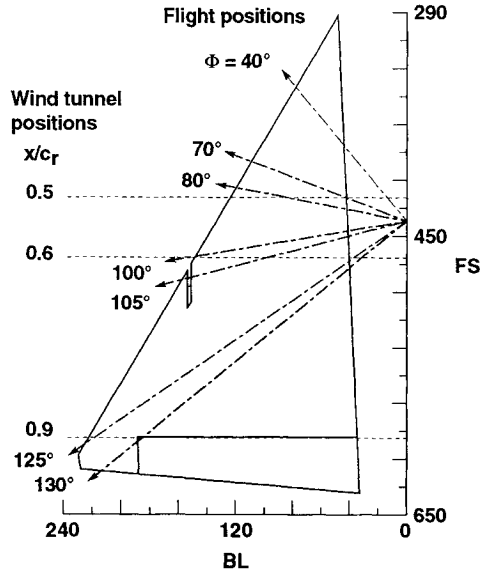

Fig. 13 Spatial relationship between Φ and wind-tunnel longitudinal vapor-screen locations on left wing.

and 7 in., respectively. Figure 10c shows the distance to these vortex features from the local leading edge along the light-sheet footprint as a function of light-sheet position angle for both data sets. Similarly, good agreement is noted between the sets of l and r, with a maximum local error of 9 and 7 in., respectively.

Comparisons

Surface Pressure

Figures 11a (α = 14.9 deg), 11b (α = 17.0 deg), and 11c (α = 18.6 deg) are used to compare surface pressures with

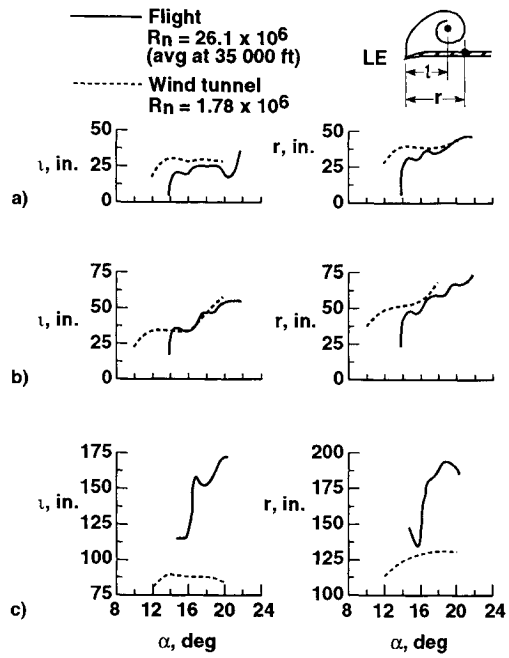

Fig. 14 Vapor-screen vortex-system characteristics based on wind-tunnel and flight-test results. a) Φ = 80 deg, x/c_r = 0.50, b) Φ = 100 deg, x/c_r = 0.60, and c) Φ = 125 deg, x/c_r = 0.90.

vortex-core tracks. Figure 11a shows good correlation over the middle part of the wing between the core tracks and the suction pressure peaks, including the second peak of belt-set 3. (Note that in order to compare these two different kinds of results, the pressure-port locations associated with the peak surface-pressures must be used.) Figures 11b and 11c also show reasonably good correlation between the two data sets, and the agreement extends more forward on the wing. This second finding is associated with the core of this dominant, single-vortex system becoming determinable at the more forward positions on the wing at the higher α.

Surface Oil-Flow Patterns

The surface oil-flow on this cambered, round-edged wing is complex in the α range from 13 to 19 deg, due to the existence of vortex systems both inboard and outboard of the wing slot. In a comparison of the reattachment point locations determined from the oil flow and those from the vapor-screen images inboard of the slot,[1] the overall agreement in both number of vortices detected and their placement is generally good. As an example, Fig. 12 (at α = 19 deg) shows the agreement between the two techniques for the dominant-vortex reattachment-lines near the FS 490 and BL 100. This figure also shows the core track to be well-positioned with respect to the streak lines.

The oil-flow portion of this figure, plus others from Ref. 1, indicate that the seemingly small distortions in wing leading-edge geometry, i.e., access straps, could well be the cause of the multiple vortices observed. This is consistent with the observations made in Ref. 13 from wind-tunnel and flight-test results of the F-106B aircraft having a leading-edge vortex flap.

Wind-Tunnel Results

In order to compare flight and wind-tunnel derived vortex features, it is first necessary to determine which data sets should be compared. Figure 13 shows the relationship between the rotating system used in-flight and the longitudinally transversing system used in the wind tunnel on a 5% scaled F-106 model. (Note the model had a smooth left wing, i.e., no access straps modeled.) Based on this figure, flight data at nominal Φ values of 80, 100, and 125 deg were compared

with tunnel data at $0.5c_r$, $0.6c_r$, and $0.9c_r$; respectively. The results are shown in Fig. 14 in terms of full-scale values. There the effect of Reynolds number on the vortex features between high-altitude flight and wind tunnel is seen to be small over the forward portion of the wing where only a single vortex system is generated for $\alpha \geq 14.8$ deg. Hence, vortex-system locations determined in the wind tunnel can give a reasonably good estimate of flight values for α from 16 to 20 deg. Valid comparisons over the aft part of the wing were not possible due to an insufficiency of the vapor-screen coverage in-flight.

Conclusions

A flight research experiment was conducted on the F-106B aircraft using a rotating vapor-screen and surface techniques in order to study the vortical flow and gain insight into the origination of the multiple-primary wing vortex-systems determined previously. The results of that study and comparisons with a related wind-tunnel test lead to the following conclusions:

1) The origin of an additional vortex at moderate angles of attack is associated with an inboard movement of the first vortex and its centroid within the vortex envelope. This is construed as the vortex changing from a leading-edge separation bubble type to the more classical off-surface type. In addition, the envelope of the first vortex is noted to develop a reflex toward the leading edge. Outboard of this region a second vortex system emerges. The cause of this seems to be associated with some fluid dynamic or some geometrical distortion.

2) From the core- and reattachment-line surface-tracks, it has been noted that additional vortex systems seem to either point to or be influenced in some way by the access straps on the wing leading edge. Thus, likely sources of the multiple vortices observed in flight are the flow disturbances associated with these straps.

3) Increasing the Reynolds number, through either an altitude or Mach number change, generally delays or suppresses large-scale separation and promotes the formation of multiple vortices. Conversely, decreasing the Reynolds number leads to large-scale, organized flow separation to begin on the wing at the lower test angles of attack. This separation reduces the number of vortex systems present, by reducing the influence of the leading-edge disturbances (access straps), and causes the outermost vortex system to be more inboard. These features are seen from both the vapor-screen images and the resulting surface track summaries.

4) Comparisons of vapor-screen determined vortex-core tracks and the surface location(s) of suction-pressure peaks(s) showed there to be good agreement for both single and multiple vortex test results.

5) A comparison of vapor-screen reattachment-point tracks with oil-flow pattern showed good agreement at angle of attack = 19 deg. In addition, analysis of the surface pattern has identified portions of the flowfield influenced by the access strap portion of the wing leading edge.

6) A Reynolds number study determined that the wind-tunnel and flight (35,000 ft) vortex-system characteristics agreed fairly well over the forward part of the wing for angle of attack ≥ 14.8 deg, where only a single vortex was present. Hence, vortex-system locations determined in the wind tunnel give a reasonably good estimate of the flight values for angles of attack from 16 to 20 deg. Valid comparisons over the aft part of the wing were not possible due to an insufficiency of the vapor-screen coverage in-flight.

References

[1]Lamar, J. E., Brandon, J., Stacy, K., Johnson, T. D., Jr., Severance, K., and Childers, B. A., "Leading-Edge Vortex-System Details Obtained on F-106B Aircraft Using a Rotating Vapor-Screen and Surface Techniques," NASA TP-3374, Nov. 1993.

[2]Lamar, J. E., Hallissy, J. B., Frink, N. T., Smith, R. H., Johnson, T. D., Jr., Pao, J.-L., and Ghaffari, F., "Review of Vortex Flow Flight Projects on the F-106B," AIAA Paper 87-2346, Aug. 1987.

[3]Lamar, J. E., and Johnson, T. D., Jr., "Sensitivity of F-106B Leading-Edge-Vortex Images to Flight and Vapor-Screen Parameters," NASA TP-2818, June 1988.

[4]Maltby, R. L., "Flow Visualization in Wind Tunnels Using Indicators," AGARDograph 70, April 1962.

[5]Campbell, J. F., and Chambers, J. R., "Patterns In the Sky—Natural Visualization of Aircraft Flow Fields," NASA SP 514, 1994.

[6]Lamar, J. E., *In-Flight and Wind Tunnel Leading-Edge Vortex Study on the F-106B Airplane*, NASA CP 2416, Vol. I, July 1986, pp. 187–210.

[7]Wood, R. M., and Watson, C. B., "Study of Lee-Side Flows over Conically Cambered Delta Wings at Supersonic Speeds," NASA TP 2660, Pt. 1, July 1987.

[8]Dimotakis, P. E., and Brown, G. L., "The Mixing Layer at High Reynolds Number: Large-Structure Dynamics and Entrainment, *Journal of Fluid Mechanics*, Vol. 78, Dec. 1976, pp. 535–560.

[9]Pierrehumbert, R. T., and Widnall, S. E., "The Structure of Organized Vortices in a Free Shear Layer," *Journal of Fluid Mechanics*, Vol. 102, Jan. 1981, pp. 301–313.

[10]Walatka, P. P., Clucas, J., McCabe, R. K., Plessel, T., and Potter, R., "FAST 1.0 User Guide," NASA Ames Research Center, RND-92-015, Moffett Field, CA, Nov. 1992.

[11]Werlé, H., "Aperçu sur les Possibilités Expérimentales du Tunnel Hydrodynamique a Visualization de l'O.N.E.R.A.," ONERA TN 48, 1958.

[12]Gregoriou, G., "Modern Missile Design for High Angle-of-Attack," AGARD-LS-121/5, March 1982.

[13]Hallissy, J. B., Schoonover, W. E., Jr., Johnson, T. D., Jr., and Brandon, J. M., "Wind-Tunnel Investigation of the Multiple Vortex System Observed in Flight Tests of the F-106B Vortex Flap Configuration," NASA TP 3322, Dec. 1993.